Journal of Zhejiang University SCIENCE A
ISSN 1673-565X (Print); ISSN 1862-1775 (Online)
www.zju.edu.cn/jzus; www.springerlink.com
E-mail: jzus@zju.edu.cn

Deformation-based freeform feature reconstruction in reverse engineering*

Qing WANG†, Jiang-xiong LI†‡, Ying-lin KE

(*State Key Lab of Fluid Power Transmission and Control, Zhejiang University, Hangzhou 310027, China*)

†E-mail: uphover@163.com; ljxiong@zju.edu.cn

Received Mar. 31, 2008; revision accepted June 24, 2008

Abstract: For reconstructing a freeform feature from point cloud, a deformation-based method is proposed in this paper. The freeform feature consists of a secondary surface and a blending surface. The secondary surface plays a role in substituting a local region of a given primary surface. The blending surface acts as a bridge to smoothly connect the unchanged region of the primary surface with the secondary surface. The secondary surface is generated by surface deformation subjected to line constraints, i.e., character lines and limiting lines, not designed by conventional methods. The lines are used to represent the underlying information of the freeform feature in point cloud, where the character lines depict the feature's shape, and the limiting lines determine its location and orientation. The configuration of the character lines and the extraction of the limiting lines are discussed in detail. The blending surface is designed by the traditional modeling method, whose intrinsic parameters are recovered from point cloud through a series of steps, namely, point cloud slicing, circle fitting and regression analysis. The proposed method is used not only to effectively and efficiently reconstruct the freeform feature, but also to modify it by manipulating the line constraints. Typical examples are given to verify our method.

Key words: Freeform feature, Surface deformation, Fishbone structure, Character line, Limiting line, Reverse engineering
doi:10.1631/jzus.A0820244 **Document code:** A **CLC number:** TP391

INTRODUCTION

Reverse engineering, as the most popular methodology, converts low-level geometric information generally represented by point cloud position and their differential geometric attributes to high-level information, such as design methods, functional principles, engineering constraints and aesthetic evaluations. Surface reconstruction is one of the most important steps in reverse engineering. Currently, surface reconstruction process is mainly focused on primary features (Eck and Hoppe, 1996; Várady *et al.*, 1997; Benkő *et al.*, 2001; Huang and Menq, 2002; Weiss, 2003; Ke *et al.*, 2006), such as natural quadric surface, regular swept surface and freeform surface. However, there is a little research on the reconstruction of freeform feature, i.e., secondary freeform feature (Fontana *et al.*, 2000). Corresponding to local shape modifications of a given primary surface, freeform features are widely used for aesthetical aspects of various industrial products, such as car components, home appliances, etc.

Fontana *et al.*(2000) characterized a freeform feature as a local modification of a surface, which could be executed by three operations: adding, substituting and removing a region. They concentrated on the deformation and elimination of surfaces, and presented a classification of freeform features according to the designer's requirement for aesthetic purposes. Renner *et al.*(1998) suggested a high-level description of large, primary surfaces and dependent feature elements, and reconstructed surface models based on point cloud fitting. In their method, freeform feature was regarded as the primary surface and generated by

‡ Corresponding author
* Project supported by the National Natural Science Foundation of China (No. 50575098) and China Postdoctoral Science Foundation

point cloud fitting. Vergeest *et al.*(2001a; 2001b) defined a parameter-based formalism: freeform features were formulated as a map from a parameter domain to a subset of the Euclidean space, and applied it to the fitting of freeform features from digitized points. Song *et al.*(2005) further implemented the freeform feature modification based on intrinsic parameters by means of deformable freeform feature templates. To verify the method, they gave the parameterization of the bump, hole and ridge features. Au and Yuen (1999) investigated template-based freeform feature reconstruction in reverse modeling of mannequin for garment design. Wang (2005) further presented a novel parameterization approach for human bodies. Using this method, surface models of human body could be efficiently constructed and a new model could be generated by modifying the parameterization. Catalano *et al.*(2002) pointed out that defining freeform feature as parametric components could be used for some specific objects in reverse engineering, but hardly for the general products. Therefore, character line and limiting line as the defining parameters of freeform feature were used in (Fontana *et al.*, 1999; Pernot *et al.*, 2002). Panchetti *et al.*(2008) applied the character lines extracted from images of the object to recovery of complex shapes in meshes.

As one type of freeform features, substitution feature can be defined by a surface assembly technique. First, the local region of a given primary surface is substituted by a new secondary surface. Then, the primary unmodified regions and the secondary surface are connected by a blending surface. The secondary surface and the blending surface jointly compose substitution feature. According to Fontana's definition of detail features, substitution feature in our method should be a subset of free form δ-features, but it is not included in Fontana *et al.*(2000)'s taxonomy. Substitution features is classified to three types, i.e., border, internal and channel, depending on its topological position relatively to the boundary of the primary surface. In conventional design, substitution features are constructed through a series of operations such as trimming and blending. The intersection curve of the primary and secondary surfaces is substituted by the blending surface, i.e., the intersection curve disappears in the physical part. Therefore in reverse modeling the boundary information of the secondary surface is unavailable where the point cloud is acquired from the physical part. Since the boundary condition is not considered in the common surface fitting methods, the intersection curve of the given primary surface and the reconstructed secondary surface is also distortion.

In this paper, we present an interactive approach, integrated reverse engineering with forward engineering for the substitution feature reconstruction. The secondary surface is reconstructed by curve-driven deformation, in which character line and limiting line are used. The character line depicts the main shape of the feature, and the limiting line describes the boundary of the influence region of the primary surface, which is modified by the insertion of the secondary surface. From an implementation point of view, they are both used as line constraints in the deformation process. The blending surface is constructed with the blending parameters extracted from point cloud. The overall work flow of substitution feature reconstruction is shown in Fig.1. For convenience, point cloud associated with secondary surface and blending surface are denoted as objective point cloud and blending point cloud, respectively. Theoretically, the maximum principal curvature (MPC) values at the blending region are significantly greater than those at the primary surface and the secondary surface. Therefore, by classifying the MPC values of the point cloud, the major blending region can be separated from the point cloud. The point cloud subsets associated with the primary surface and the secondary surface are then obtained. The segmen-

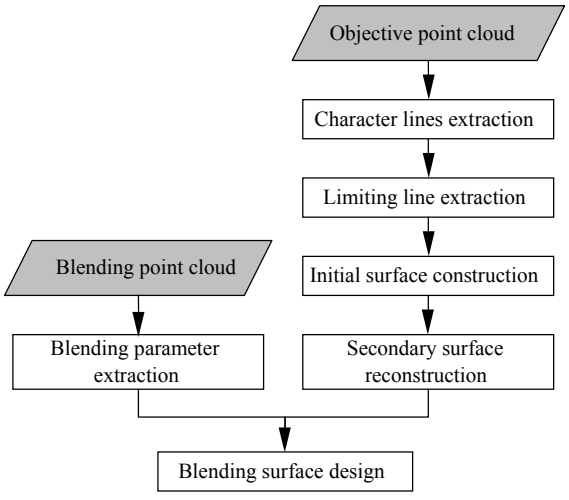

Fig.1 Flowchart of secondary surface reconstruction and blending surface design

tation process of the blending region is not concretely described here, interested readers can refer to (Ke *et al.*, 2006). In this paper, we assume that the objective point cloud and the blending point cloud have been segmented and the primary surface has been reconstructed.

This paper is organized as follows. In Section 2, we consider shape modification of non-uniform rational B-splines (NURBS) surface with different constraints by using the force density method (FDM). In Section 3 and Section 4, the extraction and utility of character lines and limiting lines are discussed, respectively. In Section 5 and Section 6, the reconstruction process of secondary surface and blending surface are described, respectively. In Section 7, two typical examples are given. In Section 8, we conclude this paper and point out future work.

FDM-BASED SURFACE MODIFICATION

Preliminaries

FDM proposed by Schek (1974) is used in form finding analysis of pin-joint network consisting of cables or bars originally. Léon and Trompette (1995), Léon and Veron (1997), Guillet and Léon (1998) and Pernot *et al.*(2003) applied FDM to the field of shape modification. Pernot *et al.*(2006) further applied it to filling holes in meshes.

Given an initial surface, a bar network with initial static equilibrium state is coupled with the control polyhedron of a surface represented by NURBS (Fig.2). Node of the bar network fixed as boundary condition is called the 'fixed node', otherwise the 'free node'. Similarly, bar connected with two fixed nodes is the fixed bar, otherwise the free bar. This bar network can provide the isotropic or anisotropic behavior of the deformation by setting a different force density to each bar. To meet different requirements, many deformation mechanisms based on the bar network, such as force variations minimization, force minimization, etc., are used to the shape modeling. A set of functional and aesthetic design constraints depicted by character lines or limiting lines are enforced to the surface deformation process. The constraints are converted into position, tangency and normal conditions by sampling methods. Design constraints enforced on the surface cause a new static equilibrium state of the bar network, thus resulting in a new surface shape. Positions of the free nodes are recomputed by solving a linear system. It means that we can efficiently obtain a deformed surface by solving a linear system. In addition, the deformation based on the physical model (a bar network) can guarantee the quality of the result. For these reasons, FDM-based shape modification is applied to the secondary surface reconstruction.

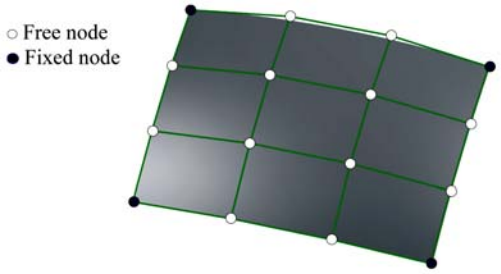

Fig.2 Control polyhedron of surface couple with a bar network

Deformation engine

We consider four minimizations as deformation engines, i.e., forces, forces variation, bar lengths and nodes displacement. These minimization problems are formulated as a unified mathematical form by using the nodes perturbation. So it is convenient to obtain a multiple combination of the minimization models which are used to satisfy the various shape requirements. Shape modification of curves and surfaces in NURBS form with different constraints can be represented with a quadratic form. Therefore, the objective functions of deformation are expressed as

$$\begin{aligned} &\min \psi(\boldsymbol{\varepsilon}) = \min\left(\frac{1}{2}\boldsymbol{\varepsilon}^{\mathrm{T}}\boldsymbol{G}\boldsymbol{\varepsilon} + \boldsymbol{H}\boldsymbol{\varepsilon}\right), \\ &\text{s.t. } C_j(\boldsymbol{\varepsilon}) = 0 \ \ (j = 0, 1, \ldots, l), \end{aligned} \tag{1}$$

where

$$\boldsymbol{G} = \begin{bmatrix} \boldsymbol{G}_x & \boldsymbol{0} & \boldsymbol{0} \\ \boldsymbol{0} & \boldsymbol{G}_y & \boldsymbol{0} \\ \boldsymbol{0} & \boldsymbol{0} & \boldsymbol{G}_z \end{bmatrix} \quad \text{and} \quad \boldsymbol{H} = \begin{bmatrix} \boldsymbol{H}_x^{\mathrm{T}} & \boldsymbol{H}_y^{\mathrm{T}} & \boldsymbol{H}_z^{\mathrm{T}} \end{bmatrix}$$

denote matrices of deformation engine, $\boldsymbol{\varepsilon} = \begin{bmatrix} \boldsymbol{\varepsilon}_x^{\mathrm{T}} & \boldsymbol{\varepsilon}_y^{\mathrm{T}} & \boldsymbol{\varepsilon}_z^{\mathrm{T}} \end{bmatrix}^{\mathrm{T}}$ denotes nodes variation vector, $\boldsymbol{\varepsilon}_x$, $\boldsymbol{\varepsilon}_y$ and $\boldsymbol{\varepsilon}_z$ indicate perturbation vectors of nodes con-

nected with free bars in coordinate axis directions, respectively. All the objective functions have the same form but different $\boldsymbol{G}$ and $\boldsymbol{H}$, therefore a unified numerical method such as Lagrange multiplier and penalty function method can be used to solve Eq.(1).

In this paper, the notation $\boldsymbol{D}_{\mathrm{ff}}=\boldsymbol{C}_{\mathrm{fb}}^{\mathrm{T}}\boldsymbol{Q}\boldsymbol{C}_{\mathrm{fb}}$, where $\boldsymbol{Q}$ is the force density matrix and $\boldsymbol{C}_{\mathrm{fb}}$ is the branch-node matrix. The matrices $\boldsymbol{f}_{\mathrm{fb}x}$, $\boldsymbol{f}_{\mathrm{fb}y}$ and $\boldsymbol{f}_{\mathrm{fb}z}$ are loaded forces matrices in coordinate axis directions, respectively. Regarding the specification in detail can refer to (Schek, 1974; Pernot *et al.*, 2003).

1. Force variations minimization

The shape is obtained by minimizing the change of external loaded forces in the least-square sense. Only the forces of the nodes connected with free bars are changeable, so the objective function is expressed as

$$\begin{aligned}\psi(\Delta\boldsymbol{f})=\Delta\boldsymbol{f}_{\mathrm{fb}}^{\mathrm{T}}\Delta\boldsymbol{f}_{\mathrm{fb}}=\Delta\boldsymbol{f}_{\mathrm{fb}x}^{\mathrm{T}}\Delta\boldsymbol{f}_{\mathrm{fb}x}+\Delta\boldsymbol{f}_{\mathrm{fb}y}^{\mathrm{T}}\Delta\boldsymbol{f}_{\mathrm{fb}y}\\+\Delta\boldsymbol{f}_{\mathrm{fb}z}^{\mathrm{T}}\Delta\boldsymbol{f}_{\mathrm{fb}z}\rightarrow\min.\end{aligned}\tag{2}$$

According to the fundamental formulae of FDM, we have $\boldsymbol{G}_x=\boldsymbol{G}_y=\boldsymbol{G}_z=\boldsymbol{D}_{\mathrm{ff}}^{\mathrm{T}}\boldsymbol{D}_{\mathrm{ff}}$ and $\boldsymbol{H}_x=\boldsymbol{H}_y=\boldsymbol{H}_z=\boldsymbol{0}$. Similar to the minimization of the surface energy variations, the force variations minimization tends to minimize the surface shape variations.

2. Forces minimization

The shape is obtained by minimizing the external loaded forces in the least-square sense. As the reason mentioned above, the objective function is expressed as

$$\psi(\boldsymbol{f})=\boldsymbol{f}_{\mathrm{fb}}^{\mathrm{T}}\boldsymbol{f}_{\mathrm{fb}}=\boldsymbol{f}_{\mathrm{fb}x}^{\mathrm{T}}\boldsymbol{f}_{\mathrm{fb}x}+\boldsymbol{f}_{\mathrm{fb}y}^{\mathrm{T}}\boldsymbol{f}_{\mathrm{fb}y}+\boldsymbol{f}_{\mathrm{fb}z}^{\mathrm{T}}\boldsymbol{f}_{\mathrm{fb}z}\rightarrow\min.\tag{3}$$

So $\boldsymbol{G}_x=\boldsymbol{G}_y=\boldsymbol{G}_z=\boldsymbol{D}_{\mathrm{ff}}^{\mathrm{T}}\boldsymbol{D}_{\mathrm{ff}}$, $\boldsymbol{H}_x=\boldsymbol{D}_{\mathrm{ff}}^{\mathrm{T}}\boldsymbol{f}_{\mathrm{fb}x}$, $\boldsymbol{H}_{\mathrm{y}}=\boldsymbol{D}_{\mathrm{ff}}^{\mathrm{T}}\boldsymbol{f}_{\mathrm{fb}y}$, and $\boldsymbol{H}_z=\boldsymbol{D}_{\mathrm{ff}}^{\mathrm{T}}\boldsymbol{f}_{\mathrm{fb}z}$. Similar to minimizing the membrane strain energy of shape, the forces minimization tends to generate a minimal surface.

3. Bar lengths minimization

The shape is obtained by minimizing the length of each bar of the network in the least-square sense, where the bars are rigid and the variations of bar length need to conquer the strains, i.e., force density. The objective function is expressed as

$$\psi(\boldsymbol{l})=\boldsymbol{l}^{\mathrm{T}}\boldsymbol{Q}\boldsymbol{l}=\boldsymbol{u}^{\mathrm{T}}\boldsymbol{Q}\boldsymbol{u}+\boldsymbol{v}^{\mathrm{T}}\boldsymbol{Q}\boldsymbol{v}+\boldsymbol{w}^{\mathrm{T}}\boldsymbol{Q}\boldsymbol{w}\rightarrow\min,\tag{4}$$

where the notion $\boldsymbol{l}$ is the vector of bar lengths and $\boldsymbol{u}$, $\boldsymbol{v}$, $\boldsymbol{w}$ are the coordinate difference matrices of the nodes in coordinate axis direction, respectively. So $\boldsymbol{G}_x=\boldsymbol{G}_y=\boldsymbol{G}_z=\boldsymbol{I}$, $\boldsymbol{H}_x=\boldsymbol{f}_{\mathrm{fb}x}$, $\boldsymbol{H}_y=\boldsymbol{f}_{\mathrm{fb}y}$ and $\boldsymbol{H}_z=\boldsymbol{f}_{\mathrm{fb}z}$. This criterion tends to minimize the length of a curve or the area of a surface without taking into account the initial shape.

4. Nodes displacement minimization

The surface is obtained by minimizing the nodes displacement in the least-square sense. The objective function is expressed as

$$\psi(\boldsymbol{\varepsilon})=\boldsymbol{\varepsilon}^{\mathrm{T}}\boldsymbol{\varepsilon}=\boldsymbol{\varepsilon}_x^{\mathrm{T}}\boldsymbol{\varepsilon}_x+\boldsymbol{\varepsilon}_y^{\mathrm{T}}\boldsymbol{\varepsilon}_y+\boldsymbol{\varepsilon}_z^{\mathrm{T}}\boldsymbol{\varepsilon}_z\rightarrow\min.\tag{5}$$

So $\boldsymbol{G}_x=\boldsymbol{G}_y=\boldsymbol{G}_z=\boldsymbol{I}$ and $\boldsymbol{H}_x=\boldsymbol{H}_y=\boldsymbol{H}_z=\boldsymbol{0}$. This criterion tends to minimize the surface displacement.

Regarding the specification of position, tangency and normal vector constraints, refer to (Welch and Watkin, 1992; Hu *et al.*, 2001). Since the continuity between the secondary surface and the primary surface is guaranteed by the blending surface, the position constraint can meet the requirement of the secondary surface reconstruction. In this situation, the equation system can be solved independently for each dimension. That is to say, the matrices $\boldsymbol{\varepsilon}$, $\boldsymbol{G}$ and $\boldsymbol{H}$ are simply replaced by the matrices $\boldsymbol{\varepsilon}_x$ ($\boldsymbol{\varepsilon}_y$, $\boldsymbol{\varepsilon}_z$), $\boldsymbol{G}_x$ ($\boldsymbol{G}_y$, $\boldsymbol{G}_z$) and $\boldsymbol{H}_x$ ($\boldsymbol{H}_y$, $\boldsymbol{H}_z$) in Eq.(1). If the position and normal vector constraints are considered as boundary conditions, the G^1 continuity between the primary and secondary surfaces also can be achieved.

CHARACTER LINE CONSTRAINTS

Specification of character lines

The set $L=\{l_i,\ 0<i<n_l\}$ of the character lines drives the shape modification, where each target leading line l_i lies on the surface resulting from deformation. A leading line l_i' is defined as the projection of l_i onto the primary surface. More precisely, $l_i'=f_{\mathrm{prj}}(l_i)\in S$, where f_{prj} is a projection operator.

Deformation process pulls the points on l_i' towards the corresponding points of l_i. Let P_{l_i} denote the points sampled from l_i. The distribution of P_{l_i} relies on sampling criterion, such as chord height, chord length and curve segment length. We adopt both chord height deviation and curve segment length as the sampling criterion (Park *et al.*, 2000). This crite-

rion results in the sampling points as few as possible while keeping the chord height deviation and the curve segment length between points less than the sampling errors δ and $k\delta$ (k is a positive value and $10 \le k \le 30$), respectively. As illustrated in Fig.3, $P_{l_i} = \{p_j,\ 0<j<n_{l_i}\} \in l_i$ are sampled from l_i with the above criterion, and their corresponding projection points are $P'_{li} = \left\{ p'_j \,\middle|\, p'_j = f_{\text{prj}}(p_j) = S(u_j, v_j),\ 0 < j < n_{li} \right\} \in l'_i$. By the same way, we can obtain the points $P_l = \{P_{li},\ 0<i<n_l\}$ of all character lines and their corresponding projection points $P'_l = \{P'_{li}, 0 < i < n_l\}$.

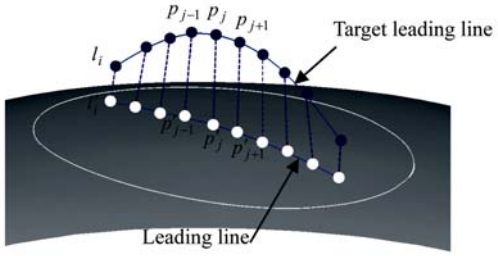

Fig.3 Character line sampling

P_l is the set of geometric points, defined by their 3D coordinates. They correspond to geometric position constraints in surface deformation process. The associated parametric points on the surface are P'_l. Let $p_j \in P_l$, $p'_j = f_{\text{prj}}(p_j) = S(u_j, v_j) \in P'_l$, then they should satisfy the following constraint equation: $\hat{S}(u_j, v_j) = S(u_j, v_j) + \boldsymbol{R\varepsilon}$ i.e., $p_j = p'_j + \boldsymbol{R\varepsilon}$ where S is a $p \times q$ degree initial surface, $\hat{S}$ is a modified surface, $\boldsymbol{R}=[R_{00}, R_{01}, \ldots R_{0m}, \ldots R_{n0}, R_{n1}, \ldots R_{nm}]$, and $R_{i,j}(u,v) = \dfrac{N_{i,p}(u) N_{j,q}(v) \omega_{i,j}}{\sum_{k=0}^{n} \sum_{l=0}^{m} N_{k,p}(u) N_{l,q}(v) \omega_{k,l}}$, $\omega_{i,j}$ is the weight, and $N_{i,p}(u)$ and $N_{j,q}(v)$ are the B-spline basis functions defined on the knot vectors $\boldsymbol{U}=[u_0, u_1, \ldots, u_n, \ldots, u_{n+p}]$ and $\boldsymbol{V}=[v_0, v_1, \ldots, v_m, \ldots, v_{m+q}]$, respectively. In this way, character lines are converted into the position constraints and lead to the initial surface deformation.

Now, we discuss the compatible condition of guaranteeing the character lines embedded into a C^2 surface. It is identical whether a unique surface curvature can be determined at each intersection point of character lines (Hermann, 1996). For convenience, we assume that: (1) the character lines are at least C^2; (2) for each intersection point of the leading lines, there exists a corresponding intersection point of the target leading lines. The assumption of the intersection point ensures that we keep the one-to-one map between P_l and P'_l. This will guarantee the valid parametrization of the character lines. Otherwise, if there is the many-to-one map between P_l and P'_l, i.e., the over-constrained condition, it will bring on the unpleasant resulting shape. Referring to Hermann (1996)'s work, we can obtain the following conclusions:

(1) Any two intersecting character lines can be embedded into a C^2 surface.

(2) Three intersection character lines can be embedded into a C^2 surface if all the tangent vectors are coplanar and not collinear at an intersection point. The curvature of the surface at the intersection point is completely determined by these character lines.

(3) If there are more than three character lines meeting at one point and they can be embedded into a C^2 surface, the curves at the intersection point should satisfy a rigidly restricting condition, which is nearly impossible to fulfill in application.

The above conclusions are used to guide us to configure the character lines. In general, the relationship of the character lines should be as simple as possible.

Configuration of character lines

In (Fontana *et al.*, 2000; Pernot *et al.*, 2002), the character lines are used to drive the surface local deformation, and give an aesthetic characterization that users want to impress on the product. In general, the degree of freedom of the surface is greater than the number of constraints, various shapes are then possible and should be accessible for the users. The shape is determined by different minimizations while satisfying the constraints. However, in our method, the character lines are used to depict the shape underlying the objective point cloud. More precisely, it is simplified as the character lines to make the objective point cloud operation easier in surface deformation. The essence of our method is to make the reconstructed surface to approximate the objective point cloud within a given error. Hence, the distribution of the extracted character lines should mostly reflect the shape of the objective point cloud.

To describe the shape of objective point cloud exactly and drive surface deformation conveniently, fishbone structure is chosen to configure the character lines. The fishbone structure, consisting of the backbone curve and the rib curves, is originally used to resample the blending regions in an anti-aliased manner (Botsch and Kobbelt, 2001). The fishbone structure is used to guide the extraction of character line in reverse modeling. The backbone curve is approximately aligned along the feature orientation, then the rib curves that branch off perpendicularly from the backbone curve are placed, as shown in Fig.4.

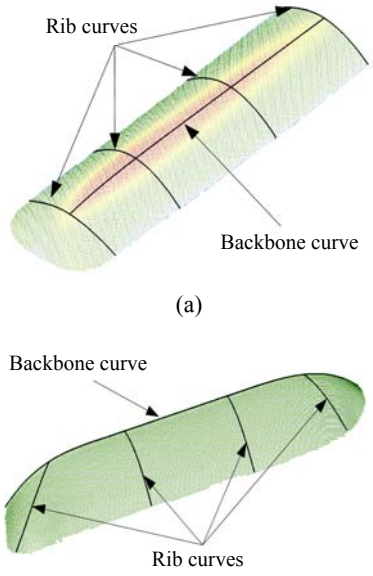

Fig.4 Fishbone structure of character lines. (a) Motorcycle part; (b) Auto part

The backbone curve is constructed by some curves modeling tools, such as crest lines extraction (Ohtake *et al.*, 2004; Belyaev and Anoshkina, 2005; Cazals and Pouget, 2005; Hildebrandt *et al.*, 2005; Yoshizawa *et al.*, 2005; Kim and Kim, 2006), boundary curve extraction (Ke and Fan, 2004), curve fitting (Piegl and Tiller, 1995) and point cloud slicing (Ke and Wang, 2006). For border features and channel features, the boundary curve is used as the backbone curve or the rib curve to meet the assembly requirement with the adjacent surfaces. A crest line (ridge or valley) is a curve on a surface formed by a set of points where the principal curvature has an extremum along its curvature line. The crest lines carry visually most prominent characteristics of a surface in a few strokes. Hence the crest line is used as the backbone curve in our method. The crest line definition involves the third and the fourth order surface derivatives. This often yields to unpleasantly rough and squiggly crest lines, since the third order derivatives are highly sensitive against unwanted surface noise (Hildebrandt *et al.*, 2005). For generating a useable curve, the initial crest line is processed by the special smoothness methods. Regarding a concrete discussion on the smoothness methods, readers are referred to (Hildebrandt *et al*., 2005). Occasionally due to the strong noise, we should construct a crest line interactively in the way that the designer sketches the initial curve by picking some points along the feature orientation, and then fitting them smoothly.

Point cloud slicing is considered as a sort of intersection between a point cloud and a plane. By using the point cloud slicing, a set of ordered planar points describing sectional profile of original object can be found (Ke *et al*., 2006). We construct a series of planes which are along and perpendicular to the backbone curve. The rib curves are then built by the point cloud slicing between the objective point cloud and the planes. Like the sectional curves in surface skinning, the number of rib curves according to the objective point cloud is not unique and is mainly determined by an approximation error. If the number of the rib curves increases, the reconstructed surface would tightly approximate the objective point cloud, while the surface quality would be poor. The spacing of rib curves is associated with the shape variation of the backbone curve. When the shape variation goes up, we should increase the rib curve number in this region, vice versa. Therefore, the rib curves selection depends on the user's experience. In application, with the approximation error estimation, we may insert some new rib curves or relocate the original rib curve on the over-error region.

In our method, the quality in accuracy of the reconstructed surface is determined by the fishbone structure, and the quality in smoothness is naturally guaranteed by the deformation criterion. Namely, the minimization should result in a fair shape with respect to the constraints. Force variations minimization and forces minimization are similar to the minimization of the energy variations and the minimization of the

membrane strain energy of the shape, respectively. With a fair initial surface, it becomes easy to obtain a high quality deformed surface by using force variations minimization or forces minimization. Therefore, we select the two minimizations to obtain the desired shape, rather than bar lengths minimization and node displacements minimization.

LIMITING LINE CONSTRAINTS

Limiting line is composed of curves on primary surface. It is treated as constraints similar to character line in surface deformation process. In this section, we first introduce a discrete model to approximately express the curve on surface, and then present an algorithm for the limiting line extraction.

Discrete curve on surface

Either implicitly or explicitly, the accurate representation of a curve on surface cannot support its manipulation conveniently (Renner and Weiss, 2004). Therefore, a discrete curve on surface (DCS) adopted in this paper is represented by a series of ordered points $C_{\mathrm{DCS}}=\{P_i\in S|i=0, 1, ..., n\}$. In our method, DCS is used to describe the initial limiting lines extracted by intersection of the curves on the objective point cloud and the primary surface. For this purpose, a series of tools are developed for DCS editing, such as shape modification and smoothness.

According to the FDM-based deformation methodology, it is convenient to implement editing tools about DCS. The abovementioned deformation criteria can be directly used to modify the shape of DCS. DCS smoothness is implemented by means of combination of forces minimization and nodes displacement minimization as follows:

$$F(\boldsymbol{\varepsilon})=\alpha\psi(\boldsymbol{f})+\beta\psi(\boldsymbol{\varepsilon})\rightarrow\min, \tag{6}$$

where $\psi(\boldsymbol{f})$ and $\psi(\boldsymbol{\varepsilon})$ indicate smoothness term and approximating term, respectively. The smoothness weight α and the approximation weight β are all positive, which determine the relationship of the smoothness term and the approximating term. Compared with the bar lengths minimization, the boundary conditions can be enforced in the forces minimization. Thus, the objective function of the forces minimization is selected as the smoothness term in our method, to obtain a desired shape in both the global smoothness and the local smoothness, as shown in Fig.5.

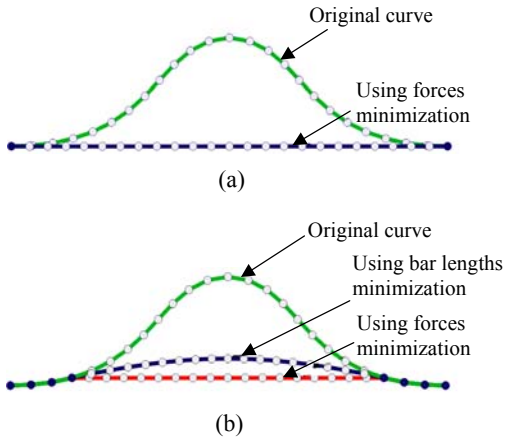

Fig.5 Smoothness model of DCS. (a) Global smoothness model; (b) Local smoothness model

Limiting line extraction

Due to a series of trimming and blending operations, it is difficult to detect the limiting line, the intersection of the primary surface and the secondary surface, from a practical product. If there is an intersection point of a curve on the secondary surface and the primary surface, it must be on the intersection curve. Based on the above lemma, an algorithm to extract the limiting line based on the objective point cloud and the primary surface is presented. The work flow of the algorithm is shown in Fig.6.

The guide curve C_{g} can be extracted directly from the boundary points of the blending point cloud (Ke and Fan, 2004), and also manually constructed on the primary surface along the direction of the blending point cloud using the DCS editing tools. Then a guide curve driven the point cloud slicing is achieved. By sampling from C_{g}, an ordered point set $P_{\mathrm{g}}=\{p_{\mathrm{g},i}|i=0, 1, ..., n\}$ is given. We create a plane E_i passing through the point $p_{\mathrm{g},i}$ and perpendicular to the tangent vector of the curve C_{g} at the point $p_{\mathrm{g},i}$. By slicing the objective point cloud with the plane E_i, planar ordered points are obtained, as illustrated in Fig.7a. Then the sectional profile c_i is generated by fitting the smoothed planar ordered point set. According to the principle of the point cloud slicing, the sectional profile c_i can be seen as a curve on the objective point cloud, i.e., a curve on the secondary surface. The section profile c_i is extended at one end close to $p_{\mathrm{g},i}$, and then a point $p_{1,i}$

is obtained by intersection of the curve c_i and the primary surface (Fig.7c). A sequence of slicing operations according to the order of the points set P_g is implemented. As a result, an ordered intersection points $P_I=\{p_{I,i}|i=0, 1, ..., n\}$ of the curves on the secondary surface and the primary surface are given. Since the guide curve C_g is similar to the limiting line in the shape and topology, the points P_I obey an even distribution. For the convenience of editing, the initial limiting line is constructed by connecting the ordered intersection points P_I with a DCS model (Fig.7d). Since the initial limiting line is extracted from the data with noise, the inevitable oscillation will appear, and then we have to interactively edit it with the tools mentioned above to obtain a smoother result (Fig.7e). For the convenience of sampling, a B-spline curve is generated by interpolating or approximating the initial limiting line. The limiting line is then generated automatically by projecting the B-spline curve onto the primary surface. An example about the limiting line extraction process of an auto part is illustrated in Fig.7 and Fig.8. The size of the bounding box is about 132.12 mm×778.32 mm×77.05 mm and the point number is 34989.

Limiting line is used as a kind of line constraint condition to drive surface deformation and also as a spine curve to construct the blending surface. Therefore the precision of the reconstructed substitution feature directly depends on the limiting line. Here, we analyze the initial limiting line extracted from a point cloud sampling from a computer aided design model of a motorcycle product. Fig.9a shows the noise-free

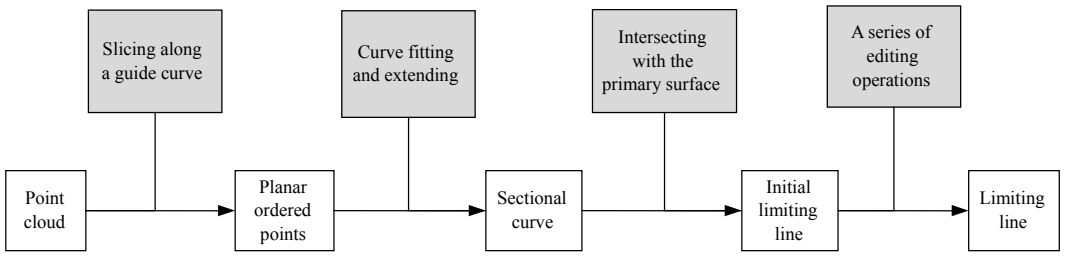

Fig.6 Flowchart of limiting line extraction

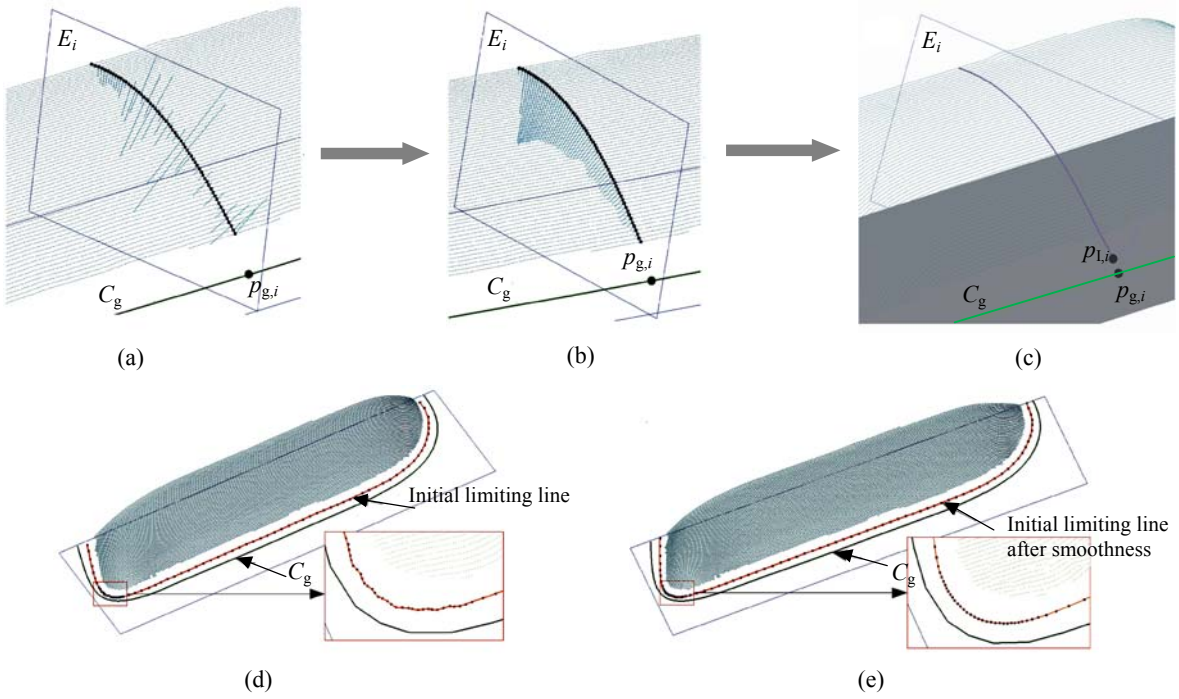

Fig.7 Limiting line extraction. (a) Planar ordered point; (b) Points after smoothing; (c) Intersection point; (d) Initial limiting; (e) Final limiting line

data (171 mm×73 mm×48 mm), in which the curve is the initial limiting line. The error histogram of the limiting line and the real intersection curve is shown in the right figure of Fig.9a, where the mean error and the maximum error are 0.117 mm and 0.216 mm, respectively. Fig.9b shows the result with adding a Gaussian noise (μ=0, σ=0.05) to the point cloud, and its error analysis histogram, where the mean error and the maximum error are 0.191 mm and 1.165 mm, respectively. From the analysis result, we observe that the extraction algorithm can meet the engineering requirement. The error is reduced once the initial limiting line is smoothed.

SECONDARY SURFACE RECONSTRUCTION

To reconstruct the secondary surface, an initial surface is provided as a deformation carrier. It should guarantee a valid parametrization. In this paper, we introduce two practical methods to construct the initial surface. Let A denote the influence region of the limiting line in the parametric domain of the primary surface. A rectangle region $A_p=\{(u, v)|u_0\le u\le u_1, v_0\le v\le v_1\}$ is then obtained by evaluating the bounding box of A along U and V directions. By enlarging the rectangle region A_p with given positive δ_u and δ_v along U and V directions, respectively, the initial surface can be

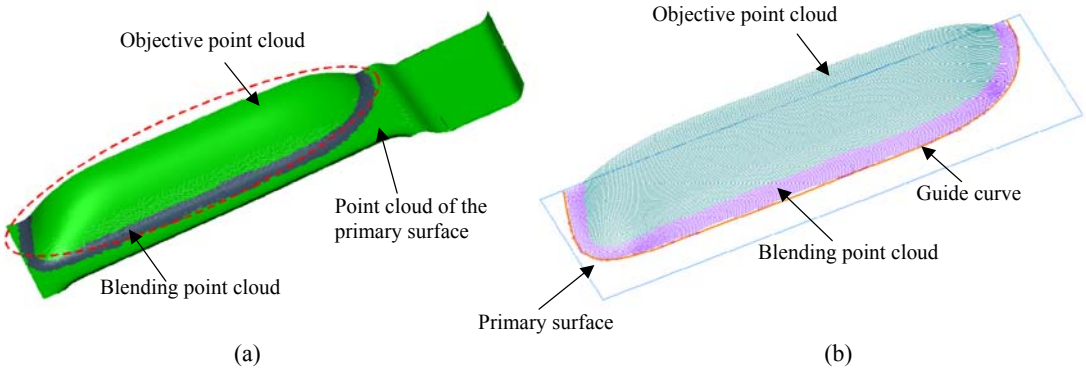

Fig.8 Point cloud of the auto part. (a) Measured data; (b) Primary surface and guide curve

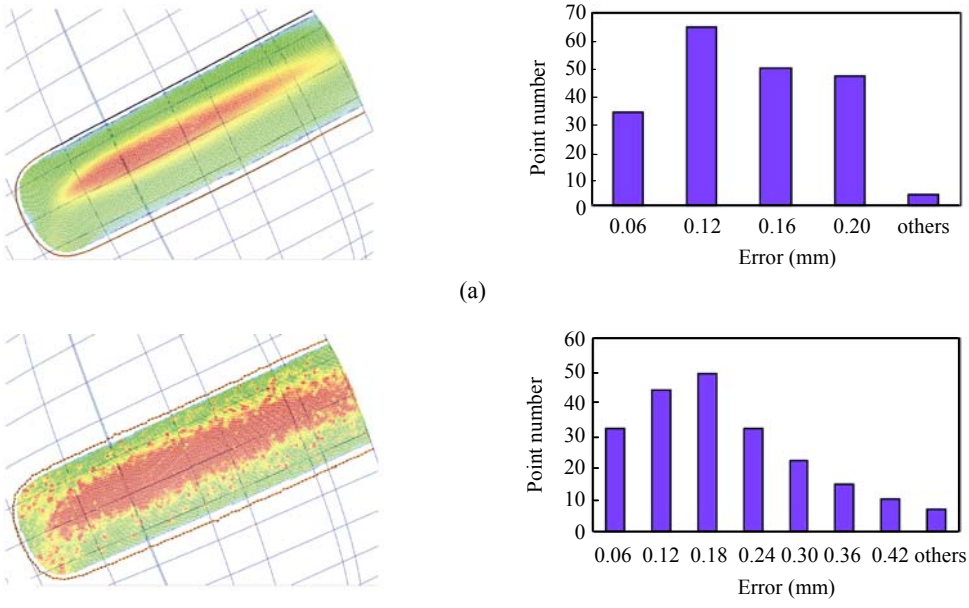

Fig.9 Error analysis. (a) Limiting line with noise-free data (left) and its error histogram (right); (b) Limiting line with noised data (left) and its error histogram (right)

automatically extracted from the primary surface according to the local support of NURBS, where $\delta_u=k(u_1-u_0)$ and $\delta_v=k(v_1-v_0)$ (k is a positive value and $0.1\leq k\leq 0.2$ generally). This method is only suitable for the case that the projection of backbone curve is nearly oriented along parametric direction of the primary surface. Another method is designed manually. First, a network of 3D curves is obtained from the primary surface, which makes the curve aligned along the backbone curves or the rib curves in parametric domain of the primary surface. Then, Gordon's method is used to construct a tensor product surface through a topologically orthogonal network of 3D curve (Piegl and Tiller, 1995).

In deformation process, all the control vertices must be used as free nodes to avoid surface aliasing effect and improve the resulting shape. According to the FDM, fixed nodes should be available as boundary conditions. We add some new nodes like the fixed nodes to the bar network. The new nodes are computed with $P_n=P_b+(P_b-P_i)$, where P_b denotes the boundary control vertex, P_i indicates the nearest inner control vertex of P_b (Fig.10).

Based on nodes configuration of the initial surface, the secondary surface is obtained by using the proposed deformation method under character line constraints and limiting line constraints. Figs.11a and11b show the reverse modeling process of the secondary surface of the auto part in Fig.8. The quality of the secondary surface is perceptible from the isophote lines in Fig.11c. As shown in Fig.11d, the error ranges from 0 to 0.995 mm, and the mean error is 0.067 mm.

BLENDING SURFACE RECONSTRUCTION

The rolling-ball blending method is used to blend two base surfaces by rolling a suitable ball with constant or variable radius and keeping the ball on both base surfaces, which are the primary surface and secondary surface in this paper. In many cases, the blending surface is created as a surface swept along a

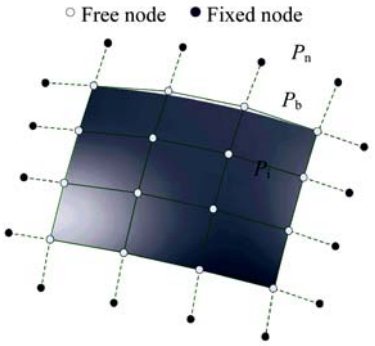

Fig.10 Nodes configuration of initial surface. The free nodes are the original nodes of the bar network, and the fixed nodes are new generation nodes

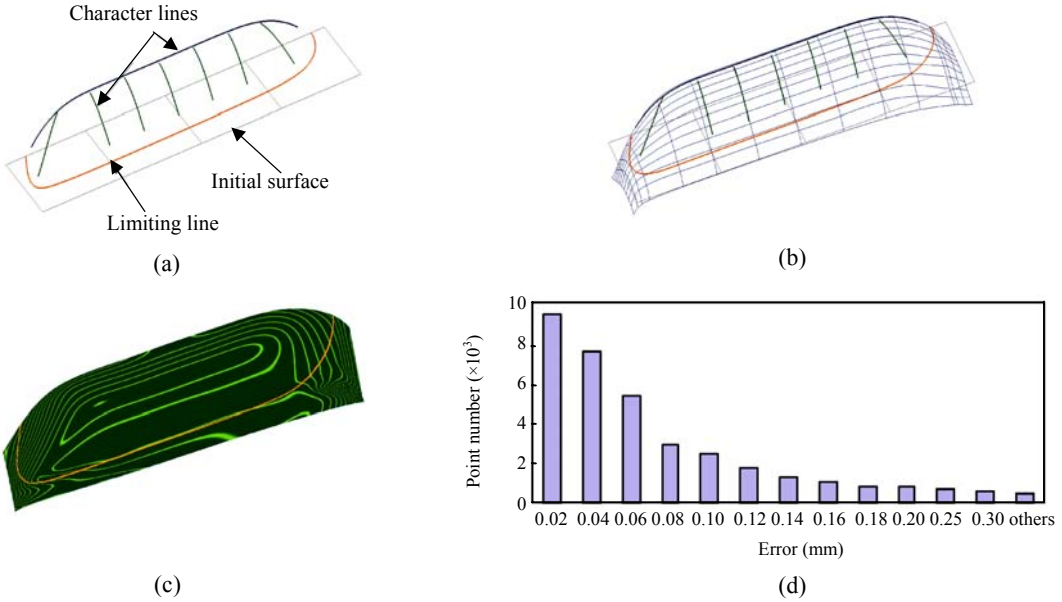

Fig.11 Secondary surface reconstruction. (a) Initial surface, character lines and limiting lines; (b) Secondary surface resulting from surface deformation; (c) Isophote of the secondary surface; (d) Error analysis of the secondary surface and the point cloud

given longitudinal trajectory, which is called the 'spine curve' (Vida *et al.*, 1994). So the spine curve and the rolling ball radius defined as the blending radius can completely express the position and the shape of the blending surface. At each point of the spine, a cross-sectional profile curve is associated with it, which locally defines the shape of the blend. For the rolling-ball blending method, the profile curve is a circular arc. Its radius is just equal to the blending radius. So we can recover the feature parameters of the blending surface by analyzing the profile curves.

Both constant radius blending and variable radius blending are taken into account in this paper. In forward design, the intersection curve between the secondary surface and the primary surface, i.e., the limiting line is often used as the spine curve to construct the blending surface. Therefore, the limiting line is used as the datum to recover the blending feature parameters in our method. First, the planar ordered points are constructed by slicing the blending point cloud with a plane perpendicular to the limiting line. The profile curve, i.e., a circular arc, is then achieved by fitting the planar ordered points. The distance function of circle can be defined as follows (Pratt, 1987):

$$d(p)=c_0(x^2+y^2)+c_1x+c_2y+c_3=0, \tag{7}$$

where the parameter vector $\boldsymbol{X}=[c_0\ c_1\ c_2\ c_3]^{\mathrm{T}}$ defines an circle. Under the quadratic normalization constraint $c_1^2+c_2^2-4c_0c_3-1=0$, $d(p)$ is a representation for the approximate geometric distance between the point (x, y) and the circle. The radius of the normalized circle is $1/|2c_0|$ and the center is $(-c_1/(2c_0), -c_2/(2c_0))$. The objective function fitting a given data point $P=\{p_0, p_1, ..., p_{n-1}\}$ is formulated as

$$f(\boldsymbol{X}) = \min \sum_{i=0}^{n-1} (d(p_i))^2. \tag{8}$$

The circle approximation, in association with the corresponding normalization constraint, is converted into an L-S (least-squared) problem and can be solved by the generalized eigenvalue method. After marching throughout the blending region along the limiting line, a set of profile curves are obtained, as illustrated in Fig.12a.

Since point cloud inevitably contains noise data, the discrete blending parameters are further evaluated by using the linear regression method. Based on the post-processing such as initial regression analysis (Fig.12b), hypothesis test, noise removing and final regression analysis (Figs.12c and 12d), we obtain the radius value for the linear variable radius blend (Ke *et al.*, 2006).

APPLICATION EXAMPLES

The proposed method has been programmed in a professional reverse modeler RE-SOFT (Ke *et al.*, 2006). Here, two practical engineering examples are given to verify the validation of our method.

Example 1

A reconstruction process of the substitution feature of an auto part is exhibited in this example, as shown in Fig.8a. The middle process has been illustrated in Figs.7, 8, 11 and 12. Fig.13a shows the reconstructed freeform feature, where the histogram of error analysis between the blending surface and the point cloud is shown in Fig.13b. The highlight analysis of the secondary surface after blending is illustrated in Fig.13c. Fig.13d shows the final reconstructed B-rep model of the auto part.

We can modify the reconstructed freeform feature by manipulating the character lines and the limiting lines, as illustrated in Fig.14. By comparing Fig.14a with Fig.11a, we can find that the limiting line and a character line are modified, while the other character lines are unchanged. The modified secondary surface is then generated based on the curve-driven deformation (Fig.14b). Fig.14c shows the final freeform feature after modification.

Example 2

The point cloud scanned from a mobile diaphragm contains 63146 scattered points, and its bounding box has a size of 12.0 mm×11.0 mm×1.0 mm, as shown in Fig.15a. The component consists of a revolution surface, a sphere surface, and 40 freeform features. The revolution surface and the sphere surface as the primary surfaces can be reconstructed from the point cloud by using the sectional features based strategy and surface feature based strategy

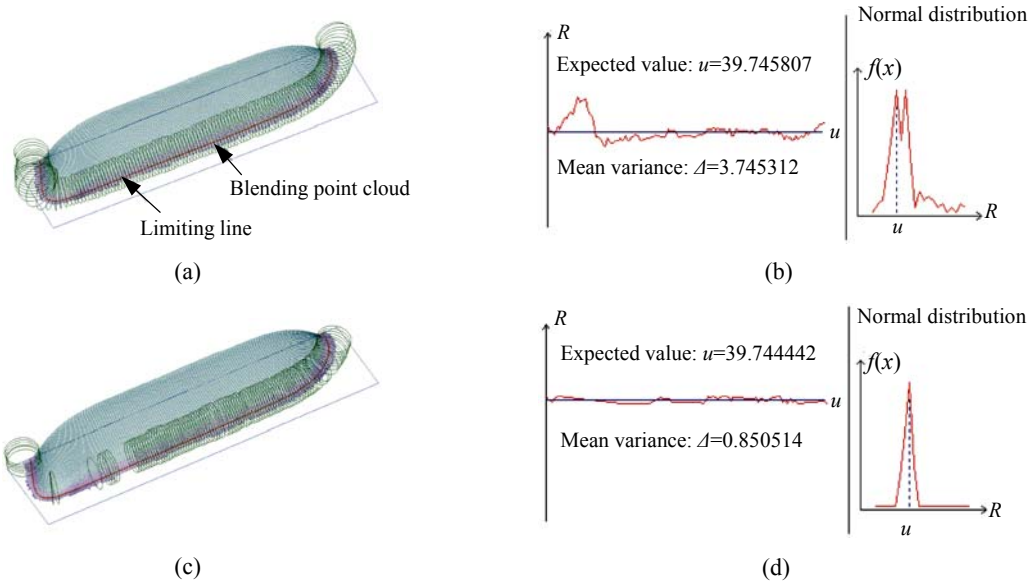

Fig.12 Regression analysis of const radius blend parameters. (a) Initial discrete blend parameter extracted from point cloud; (b) Initial regression without filtering noise; (c) Discrete blend parameter after regression analysis; (d) Final regression without filtering noisy data

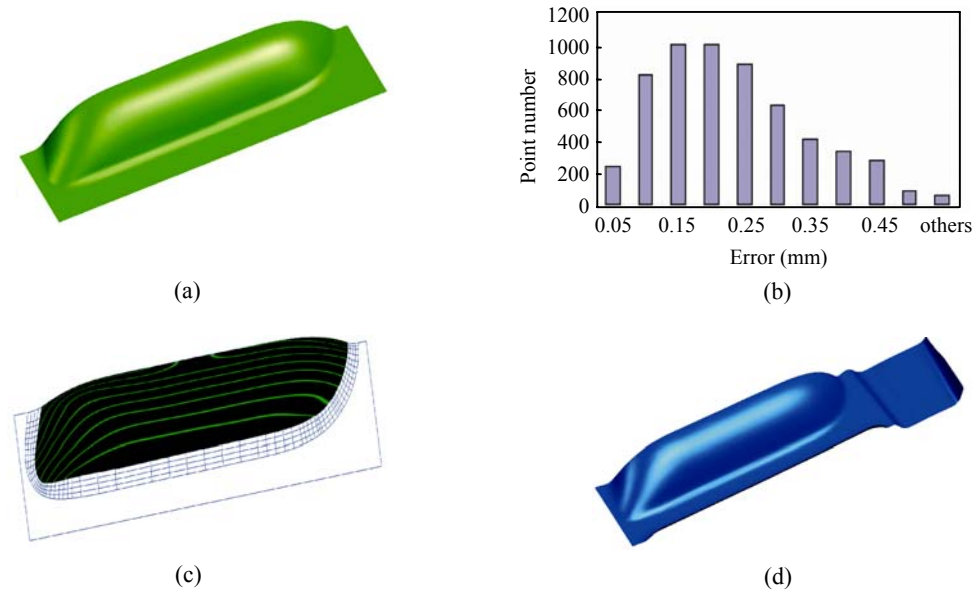

Fig.13 Freeform feature reconstruction of an auto part. (a) Freeform feature resulting from surface deformation; (b) Histogram of error analysis of blending surface and point cloud; (c) Highlight; (d) Sheet body

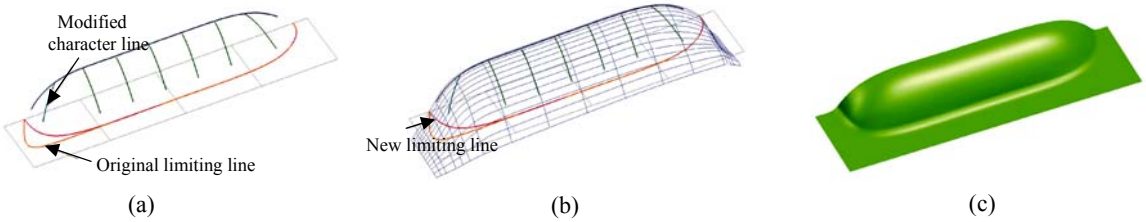

Fig.14 Modification of a reconstructed substitution feature. (a) Character lines and limiting lines after modification; (b) New secondary surface resulting from deformation; (c) New substitution feature

(Ke *et al.*, 2006), as shown in Fig.15c. Fig.16 illustrates the secondary surface reconstruction by using our method. In detail, the primary surface, the limiting line and the fishbone structure of the character lines are shown in Figs.16a, 16b and 16c. The reconstructed surface resulting from surface deformation is shown in Fig.16d. The reconstructed secondary surface after trimming along the limiting line and its highlight are illustrated in Figs.16e and 16f, respectively. Once one freeform feature is constructed, the other freeform features can be obtained by using circular array operation, where the revolution axis of the revolution surface is applied to the center of circular. The final model and its error analysis are shown in Fig.17.

CONCLUSION

A deformation-based methodology for reconstructing the substitution features is presented in this paper. By means of the character lines and the limiting lines, we construct the curve-based representation of the objective point cloud, and then the secondary surface is reconstructed based on the curve-driven deformation. The fishbone structure is introduced and applied to configure the character lines to exactly describe the shape of objective point cloud. From a curve compatibility point of view, the structure is suitable for the deformation based surface reconstruction. In the detection of the limiting line, the DCS is adopted. A series of tools for the DCS manipulation

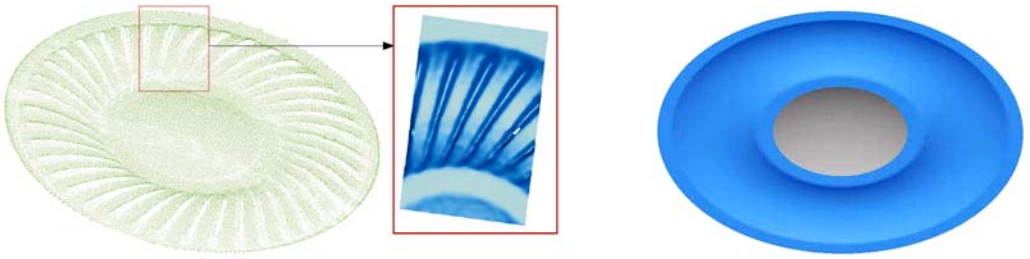

Fig.15 Mobile diaphragm. (a) Measure data; (b) Local rendering model with the substitution feature; (c) Reconstructed primary surface

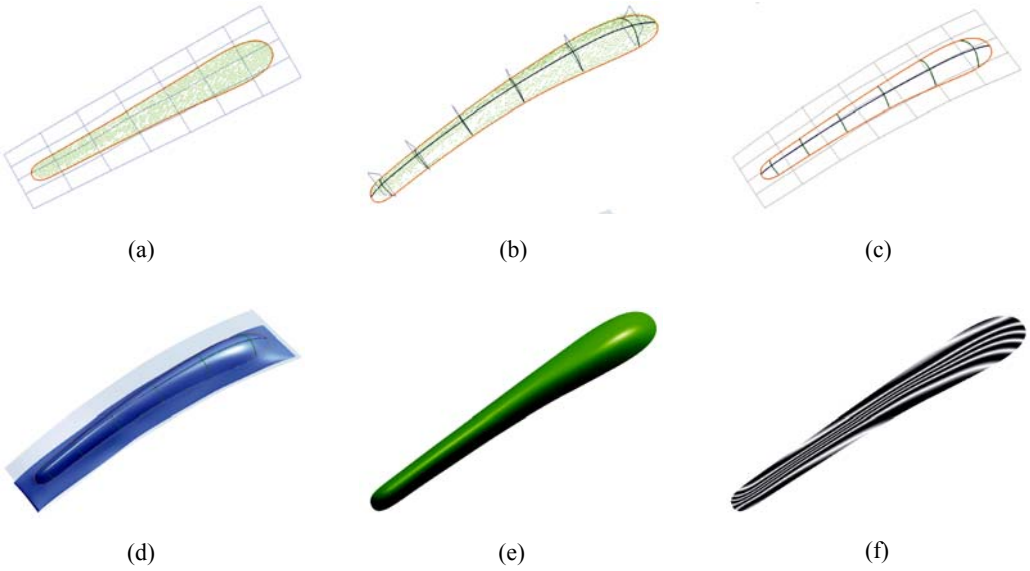

Fig.16 Secondary surface reconstruction resulting from deformation. (a) Initial surface and limiting line; (b) Fishbone structure; (c) Initial surface limiting line and character lines; (d) Reconstructed surface model; (e) Secondary surface after trimming along limiting line; (f) Highlight analysis

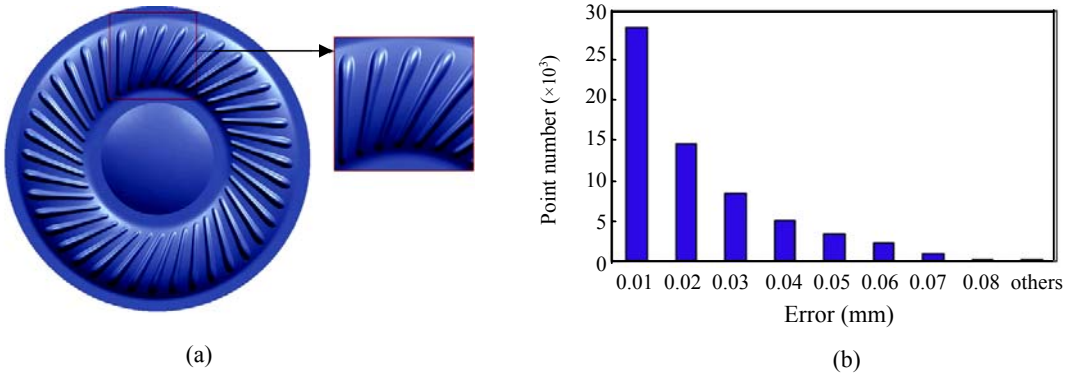

(a) (b)

Fig.17 Reconstructed model of mobile diaphragm. (a) Reconstructed surface; (b) Error histogram graph

and smoothness are developed according to the theory of the FDM-based deformation. Using this method, it is convenient to reconstruct the substitution feature and to modify the reconstructed surface by curve modification. However, our proposed method is semi-automatic. For some applications, manual operations and adjusting are adopted in the reconstruction process, such as backbone curve reconstruction, rib curves reconstruction, initial limiting line reconstruction, etc.

Many aspects need to be regarded in our future work, such as (1) enhancing the approach to ensure G^1 and/or G^2 continuity between the reconstructed primary and secondary surfaces; (2) constructing the template library about the fishbone model to fit the various objective point cloud and (3) considering the point cloud information during deformation which makes the reconstructed surface approximate each point of the point cloud.

Reference

Au, C.K., Yuen, M.F., 1999. Feature-based reverse engineering of mannequin for garment design. *Computer-Aided Design*, **31**(12):751-759. [doi:10.1016/S0010-4485(99)00068-8]

Belyaev, A., Anoshkina, E., 2005. Detection of Surface Creases in Range Data. Proceedings of the 11th IMA Conference on the Mathematics of Surfaces, Berlin, p.50-61.

Benkő, P., Martin, R.R., Várady, T., 2001. Algorithms for reverse engineering boundary representation models. *Computer-Aided Design*, **33**(11):839-851. [doi:10.1016/S0010-4485(01)00100-2]

Botsch, M., Kobbelt, L., 2001. Resampling feature and blend regions in polygonal meshes for surface anti-aliasing. *Computer Graphics Forum*, **20**(3):402-410. [doi:10.1111/1467-8659.00533]

Catalano, C.E., Falcidieno, B., Giannini, F., Monti, M., 2002. A survey of computer-aided modeling tools for aesthetic design. *Journal of Computing and Information Science in Engineering*, **2**(1):11-20. [doi:10.1115/1.1481371]

Cazals, F., Pouget, M., 2005. Topology Driven Algorithms for Ridge Extraction on Meshes. Rapport de Recherche RR5526, INRIA.

Eck, M., Hoppe, H., 1996. Automatic reconstruction of B-spline surfaces of arbitrary topological type. *Computer Graphics*, **30**(4):325-334.

Fontana, M., Giannini, F., Meirana, M., 1999. A free form feature taxonomy. *Computer Graphics Forum*, **18**(3):107-118.

Fontana, M., Giannini, F., Meirana, M., 2000. Free form features for aesthetic design. *International Journal of Shape Modeling*, **6**(2):273-302. [doi:10.1142/S0218654300000168]

Guillet, S., Léon, J.C., 1998. Parametrically deformed free-form surfaces as part of a variational model. *Computer-Aided Design*, **30**(8):621-630. [doi:10.1016/S0010-4485(98)00019-0]

Hermann, T., 1996. G^2 interpolation of free form curve networks by biquintic Gregory patches. *Computer Aided Geometric Design*, **13**(9):873-893. [doi:10.1016/S0167-8396(96)00013-1]

Hildebrandt, K., Polthier, K., Wardetzky, M., 2005. Smooth Feature Lines on Surface Meshes. Proceedings of the Third Eurographics Symposium on Geometry Processing, Vienna.

Hu, S.M., Li, Y.F., Ju, T., Zhu, X., 2001. Modifying the shape of NURBS surfaces with geometric constraints. *Computer-Aided Design*, **33**(12):903-912. [doi:10.1016/S0010-4485(00)00115-9]

Huang, J.B., Menq, C.H., 2002. Automatic CAD model reconstruction from multiple point clouds for reverse engineering. *Journal of Computing and Information Science in Engineering*, **2**(3):160-170. [doi:10.1115/1.1529210]

Ke, Y., Fan, S., 2004. Research on direct extraction of boundary from point cloud. *Chinese Journal of Mechanical Engineering*, **9**(40):116-120 (in Chinese).

Ke, Y., Wang, Q., 2006. Research on point cloud slicing technique in reverse engineering. *Journal of Computer-Aided Design and Computer Graphics*, **17**(8):1798-1802 (in Chinese).

Ke, Y., Fan, S., Zhu, W., Li, A., Liu, F., Shi, X., 2006. Feature-based reverse modeling strategies. *Computer-Aided Design*, **38**(5):485-506. [doi:10.1016/j.cad.2005.12.002]

Kim, S.K., Kim, C.H., 2006. Finding ridges and valleys in a discrete surface using a modified MLS approximation. *Computer-Aided Design*, **38**(2):173-180. [doi:10.1016/j.cad.2005.10.004]

Léon, J.C., Trompette, P., 1995. A new approach towards free-form surfaces control. *Computer Aided Geometric Design*, **12**(4):395-416. [doi:10.1016/0167-8396(94)00022-K]

Léon, J.C., Veron, P., 1997. Semi-global deformation and correction of free-form surfaces using a mechanical alternative. *The Visual Computer*, **13**(3):109-126. [doi:10.1007/s003710050093]

Ohtake, Y., Belyaev, A.G., Seidel, H.P., 2004. Ridge-valley lines on meshes via implicit surface fitting. *ACM Transactions Graphics*, **23**(3):609-612. [doi:10.1145/1015706.1015768]

Panchetti, M.H., Pernot, J.P., Véron, P., 2008. Towards Recovery of Complex Shapes in Meshes Using Shaded Images. Tools and Methods for Competitive Engineering (TMCE'08), Izmir, Turkey, p.187-198.

Park, H., Kim, K., Lee, S.C., 2000. A method for approximate NURBS curve compatibility based on multiple curve refitting. *Computer-Aided Design*, **32**(4):237-255. [doi:10.1016/S0010-4485(99)00088-3]

Pernot, J.P., Guillet, S., Léon, J.C., 2002. A Shape Deformation Tool to Model Character Lines in the Early Design Phases. Proceedings of SMI2002: International Conference on Shape Modelling and Applications. IEEE Press, Banff, Canada, p.165-172.

Pernot, J.P., Guillet, S., Léon, J.C., Falcidieno, B., Giannini, F., 2003. A New Approach to Minimizations for Shape Control during Free-form Surface Deformation. International Design Engineering Technical Conferences and Design and Automation Conference, Chicago.

Pernot, J.P., Moraru, G., Véron, P., 2006. Filling Holes in Meshes for Efficient Reverse Engineering of Products. Tools and Methods for Competitive Engineering (TMCE), Ljubljana, Slovenia, p.273-284.

Piegl, L., Tiller, W., 1995. The NURBS Book. Springer, Berlin, p.410-419, 485-496.

Pratt, V., 1987. Direct least-squares fitting of algebraic surfaces. *Computer Graphics*, **21**(4):145-152. [doi:10.1145/37402.37420]

Renner, G., Várady, T., Weiss, V., 1998. Reverse Engineering of Free-form Features. PROLAMAT 98, Trento.

Renner, G., Weiss, V., 2004. Exact and approximate computation of B-spline curves on surfaces. *Computer-Aided Design*, **36**(4):351-362. [doi:10.1016/S0010-4485(03)00100-3]

Schek, H.J., 1974. The force density method for form finding and computation of general networks. *Computer Methods in Applied Mechanics and Engineering*, **3**(1):115-134. [doi:10.1016/0045-7825(74)90045-0]

Song, Y., Vergeest, J.S.M., Bronsvoort, W.F., 2005. Fitting and manipulating freeform shapes using templates. *Journal of Computing and Information Science in Engineering*, **5**(2):86-94. [doi:10.1115/1.1875592]

Várady, T., Martin, R.R., Coxt, J., 1997. Reverse engineering of geometric models—an introduction. *Computer-Aided Design*, **29**(4):255-268. [doi:10.1016/S0010-4485(96)00054-1]

Vergeest, J.S.M., Horvàth, I., Spanjaard, S., 2001a. Parameterization of Freeform Features. Proceeding of the International Conference on Shape Modelling and Applications. IEEE Press, Genova, Italy.

Vergeest, J.S.M., Spanjaard, S., Horváth, I., Jelier, J.J.O., 2001b. Fitting freeform shape patterns to scanned 3D objects. *Journal of Computing and Information Science in Engineering*, **1**(3):218-224. [doi:10.1115/1.1419197]

Vida, J., Martin, R.R., Várady, T., 1994. A survey of blending methods that use parametric surfaces. *Computer-Aided Design*, **26**(4):341-365. [doi:10.1016/0010-4485(94)90023-X]

Wang, C.L.C., 2005. Parameterization and parametric design of mannequins. *Computer-Aided Design*, **37**(1):83-98. [doi:10.1016/j.cad.2004.05.001]

Weiss, V., 2003. Reverse Engineering Shapes by Functional Decomposition. Geometric Modelling Laboratory, Computer and Automation Research Institute, Hungarian Academy of Sciences.

Welch, W., Watkin, A., 1992. Variational surface modeling. *Computer Graphics*, **26**(2):157-166. [doi:10.1145/142920.134033]

Yoshizawa, S., Belyaev, A.G., Seidel, H.P., 2005. Fast and Robust Detection of Crest Lines on Meshes. Proceedings of the ACM Symposium on Solid and Physical Modeling. ACM Press, Cambridge, Massachusetts, p.227-232.